InP based lasers and optical amplifiers with wire-/dot-like active regions

J P Reithmaier[1], A Somers[1], S Deubert[1], R Schwertberger[1], W Kaiser[1], A Forchel[1], M Calligaro[2], P Resneau[2], O Parillaud[2], S Bansropun[2], M Krakowski[2], R Alizon[3], D Hadass[3], A Bilenca[3], H Dery[3], V Mikhelashvili[3], G Eisenstein[3], M Gioannini[4], I Montrosset[4], T W Berg[5], M van der Poel[5], J Mørk[5] and B Tromborg[5]

[1] Technische Physik, Physikalisches Institut, Universität Würzburg, Am Hubland, 97074 Würzburg, Germany
[2] D-Groupe Composants Optroniques, Thales R&T France, Domaine de Corbeville, 91404 Orsay Cedex, France
[3] Electrical Engineering Department, Technion, 32000 Haifa, Israel
[4] Dipartimento di Elettronica and PhotonLab, Politecnico di Torino, Corso Duca degli Abruzzi 24, 10129 Torino, Italy
[5] Research Center COM, Technical University of Denmark, 2800 Lyngby, Denmark

E-mail: jpreith@physik.uni-wuerzburg.de

Abstract
Long wavelength lasers and semiconductor optical amplifiers based on InAs quantum wire-/dot-like active regions were developed on InP substrates dedicated to cover the extended telecommunication wavelength range between 1.4 and 1.65 μm. In a brief overview different technological approaches will be discussed, while in the main part the current status and recent results of quantum-dash lasers are reported. This includes topics like dash formation and material growth, device performance of lasers and optical amplifiers, static and dynamic properties and fundamental material and device modelling.

(Some figures in this article are in colour only in the electronic version)

1. Introduction

The reduction of the dimensionality of electronic systems in semiconductors allows us to utilize basic quantum mechanical effects to control macroscopic material properties relevant to device applications. This idea was already realized at the beginning of the seventies by introducing quantum wells in semiconductor lasers to control the band gap by the quantum size effect and to improve the carrier confinement in growth direction. However, the ultimate lowest dimensionality will be reached by restricting the carrier movement in all three directions in quantum dot (QD)-like structures. Although this idea was born quite early in the eighties [1, 2], even before quantum well lasers had approached a final development stage, it took a long time to the demonstrate real advantages of QD laser materials, like a lower threshold current density [3], improved temperature stability of the threshold current density [4, 5] and the emission wavelength [6].

While most of the early QD work was successfully performed on GaAs substrates with laser wavelengths near 1 μm [7] down to 1.3 μm [8, 9], it was quite challenging to obtain long wavelength QD lasers. Different approaches were investigated and are still under development. In principle it is also possible to further push the emission wavelength on standard GaAs based dot systems by enlarging the InAs dot size. However, this is limited by the maximum acceptable built-in strain to about 1.35 μm before the material degrades. Only with a partial strain release by using a pseudomorphic buffer, an emission wavelength of 1.49 μm could be demonstrated recently on GaAs substrates [10].

However, due to a large lattice mismatch of the dots to the GaAs substrate and the high defect density in the buffer structure, reliability issues are much more severe.

By using InP substrates the lattice mismatch between the InAs and the substrate material can be reduced to about half of the value in comparison with GaAs. This allows much more design freedom and has the potential to extend the emission wavelength well beyond 1.5 μm. However, the dot formation process on InP and related lattice matched ternary and quaternary compounds is much more complex. The highest complexity was observed on (001) InP substrates, where a quantum wire-like [11] or dot-like formation [12] or the formation of both types is possible, depending on variations of the growth parameters [13]. Only recently, a more systematic study was reported, which shows the dot formation depends on the substrate orientation [14]. Although there was a first report on InAs/GaInAs QD lasers grown on (001) InP showing 1.9 μm laser emission at 77 K [15], many groups focused first on highly misoriented substrates, like (311)B InP [16, 17], to get a better control on the dot formation process. Unfortunately, misoriented substrates have great disadvantages in device processing, like facet cleaving and anisotropic etching. Therefore, growth on (001) InP substrates is preferred to address better the manufacturability issue.

In this paper, a brief overview is given in the first paragraph about the major growth techniques used currently for long wavelength QD structures and lasers based on InP substrates, while the main part focuses on recent results gained on dash-like material. The quantum dash (QDash) material consists of elongated, self-assembled nanostructures as seen in figure 1. A close look at the scanning electron microscope (SEM) picture in figure 1 reveals that the nanostructures resemble a dense assembly of quantum wires. However, there are many structural irregularities, which suggest the possibility of localizations and possibly a QD-like behaviour. The electronic and optoelectronic nature of the QDash structure were calculated rigorously [18] assuming a quantum wire-like density of state functions. The resultant gain functions were used to fit measured amplified spontaneous emission (ASE) spectra of a QDash amplifier. A superb fit over two orders of magnitude in the drive current and over a spectral width of 300 nm was demonstrated, while no fit could be obtained for QD gain functions. We conclude therefore that QDash gain material has indeed the properties of an assembly of quantum wires.

Another approach we have used [19] assumes elongated dots with strong quantization effects in the vertical direction and one lateral direction, while in the other lateral direction the quantization effect is weak and may not be resolved at room temperature. Although the geometry is far from an ideal dot shape, most of the advantages expected for quasi-zero-dimensional structures can be preserved and high device performances can be obtained here owing to a high dash density. Examples for lasers and optical amplifiers will be discussed.

2. Dot formation

For the formation of dot-like or dash-like islands, InAs is deposited on InP based lattice matched materials, like InGaAs, AlGaInAs or GaInAsP layers. Due to the reduced lattice mismatch between InAs and InP, the island size is slightly larger than for GaAs based QDs. Typical lateral dimensions are 20–30 nm in one direction and 20 to several 100 nm in the other direction. The height in the growth direction is of the order of 5–10 nm. Dot formation was obtained with most of the common growth techniques like solid source molecular beam epitaxy (MBE) [16], gas source MBE (GS-MBE) [17], metal organic vapour phase epitaxy (MOVPE) [20] and chemical beam epitaxy (CBE) [21]. Although some general trends are obvious, many different growth techniques were developed depending on the growth system, growth mode and substrate orientation. In the following, a brief overview is given about different growth techniques and their current status of device performance.

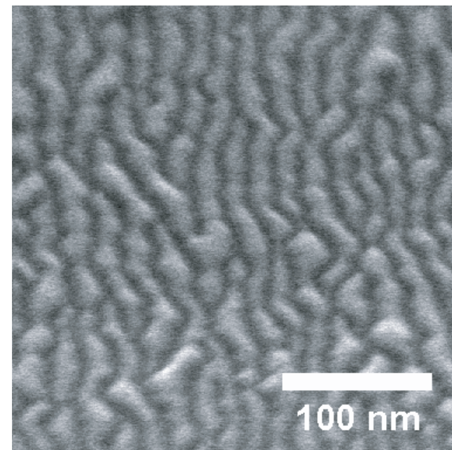

Figure 1. SEM top view of an uncapped InAs QDash sample with 5 ML InAs grown on AlGaInAs.

2.1. *Growth on high-index substrates*

Highly tilted substrates like (311)B InP offer a high density of nucleation points for island formation, which strongly reduces surface migration effects and leads to the formation of more symmetric QDs in the planar direction. Also, the dot density is relatively high, of the order of 5–10 $\times$ 10^{10} cm^{-2} [16, 22–25]. The typical geometrical dimensions are about 30–35 nm diameter and 5–6 nm height for a wavelength of 1.5 μm. The inhomogeneous linewidth broadening is quite large, with a typical value of about 100 meV and above [16, 17].

In the case of MBE growth, the dot size fluctuation could be reduced and the nucleation positions more homogeneously distributed by using an AlGaInAs buffer layer instead of an AlInAs. This seems to enhance the surface migration and promotes lateral self-ordering effects [16]. Li *et al* [16] showed a reduction of the low temperature photoluminescence linewidth from 107 to 77 meV. However, the dot density reduces from 6 $\times$ 10^{10} cm^{-2} down to 3 $\times$ 10^{10} cm^{-2}, while the dot dimensions increase to more than 50 nm in the lateral directions and 9 nm in height. As a consequence of the larger dot size, the emission energy shifts by 120 meV from 0.98 to 0.86 eV.

A further improvement in geometry control was achieved by a double cap layer technique [26], which allows truncation of the dot height. As a consequence, the height dispersion is smaller and the inhomogeneous linewidth broadening could be reduced from 70 to 50 meV at an emission wavelength of

1.5 μm. For a typical geometry with 30–35 nm diameter and a height of about 3 nm, the ground state transition is separated by about 45 meV from the first excited transition, which is approximately equivalent to one inhomogeneous linewidth.

A different approach was used by Mori *et al* [27] to control the dot size and the emission wavelength. Here, GaAs/InAs short period superlattices were grown on (411)A InP. By changing the InAs monolayer (ML) thickness and/or number of superlattice periods, the emission wavelength could be continuously tuned between 1.3 and 1.6 μm. With this technique, a minimum inhomogeneous linewidth of about 35 meV was observed at a wavelength of around 1.5 μm.

Although the basic optical performance of dot layers and the high dot density on high-index InP substrates seem favourable for obtaining dot lasers, it was difficult to achieve lasing operation at room temperature. Nishi *et al* [23] reported the first lasing operation in 1998 on an excited dot transition at 1.4 μm, while the first room temperature lasing in pulsed operation at the ground state (1.6 μm) was reported in 2001 by Saito *et al* [28] with a threshold current density of 660 A cm^{-2} in a 50 μm wide and 2.2 mm long broad-area laser.

Due to device processing problems of misoriented substrates, e.g. mirror cleaving and anisotropic etching being difficult, the main focus on laser research moved in the meantime to (001) InP substrates.

2.2. Circular dot formation on (001) InP substrates

The formation of circular dots on (001) InP is more complex, and a transition between elongated and circular dots is observed, depending on the growth mode [13]. Due to this reduced dot size control, it seems that a stronger inhomogeneous linewidth broadening is caused in comparison with dots formed on (311) InP, with measured linewidths between about 100 meV [13, 29] up to 200 meV [30].

The major problem on the road to obtaining long wavelength QD lasers on (001) InP substrates was at the beginning a low dot density of the order of 1×10^{10} cm^{-2}. However, because of the technological importance of using (001) substrates, several groups investigated the dot formation of circular shaped dots on (001) InP substrates by using different growth procedures and different epitaxial equipment (MBE, MOVPE, CBE, GS-MBE) [21, 29–34].

For example, by using a CBE system, a typical recipe for the formation of circular dots on (001) InP substrates is to deposit a few MLs of InAs on a quaternary GaInAsP layer (lattice matched to InP) and to stop the growth for half a minute under As overpressure to enhance the island formation [32]. However, on shortening the growth interruption to 5 s, elongated and preferentially oriented islands are formed [21]. A similar recipe is used by MOVPE in growing InAs dots on AlGaInAs [33]. Here a 12 s growth interruption was used after 2.5 ML InAs deposition.

To allow also emission wavelengths beyond 1.6 μm, the InAs dot layer is embedded in an InGaAs QW layer [34] as in to approaches in 1.3 μm GaAs based dot material. However, due to an increased In supply by the underlying part of the InGaAs QW layer, the dot size uniformity decreases. Qiu and Uhl [35] have used a thin GaAs intermediate layer between the InAs QD and the underlying InGaAs layer. This seems to improve

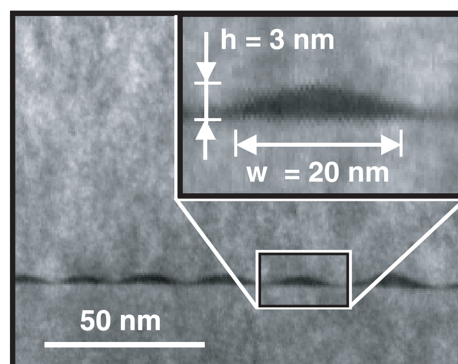

Figure 2. XTEM image of overgrown QDash test sample perpendicular to the dashes. For the formation of the QDashes, 5 ML InAs were deposited. The inset shows a magnification of a single QDash structure with the indicated dimensions [39].

the dot homogeneity by avoiding In mass transportation into the QD layer and improves the optical quality by reduced hot carrier effects, thanks to electron tunnelling injection. Continuous wave (CW) operation could be shown up to 260 K [34].

Very recently, Kim *et al* [36] reported the first room temperature laser operation at 1.5 μm in pulsed mode. The dot structures, consisting of seven stacked dot layers separated by AlGaInAs barrier layers, exhibit an improved dot density of 6×10^{10} cm^{-2} and a reduced size fluctuation (PL linewidth = 75 meV). A threshold current density of about 5 kA cm^{-2} was obtained for a 15 μm wide and 1.25 mm long ridge laser.

Further improvement of the dot density and the modal gain of lasers with circular dot material on (001) InP substrates is necessary to obtain applicable device quality including CW operation up to 85°C and reasonable low threshold current densities.

2.3. Dash formation on (001) InP substrates

In contrast to circular shaped dots grown on (001) InP, the growth of dash-like material does not need special growth interruption techniques. Due to the reduced difference in the lattice constant between InP and InAs in comparison with the InAs/GaAs system, the spontaneous nucleation in the Stransky–Krastanov growth mode is more strongly influenced by ML steps, which locally initiate nucleation and pre-define lateral growth directions.

The standard growth process is far from thermal equilibrium, resulting in time dependent growth effects. Therefore, growth interruptions, substrate temperature and flux rates have a large impact on the dash formation. In figure 1, a SEM image of an uncapped InAs QDash sample is shown, which was grown under standard conditions (As_4 overpressure, InAs growth rate of about 0.4 μm h^{-1}, substrate temperature 480°C, no growth interruption) on an $In_{0.528}Ga_{0.234}Al_{0.238}As$ lattice matched to InP by using a solid source MBE system. The elongated dots are preferentially oriented in the $[0\bar{1}1]$ direction with fluctuations in orientation and geometrical dimensions [37, 38].

In general, overgrowth with AlGaInAs could change the size and density of the dots. However, as can be seen on a cross section transmission microscope (XTEM) image in figure 2,

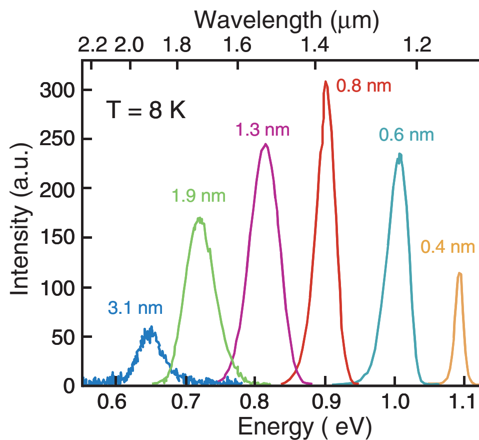

Figure 3. Low temperature PL spectra of QDash layers with different nominal InAs layer thickness as indicated.

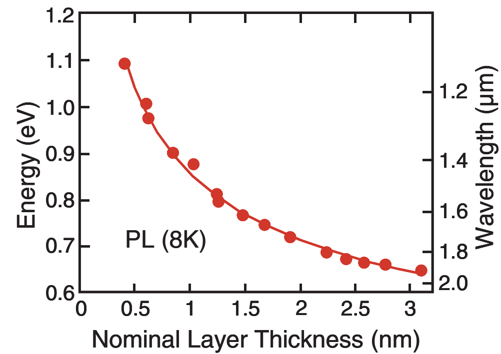

Figure 4. Luminescence energy as a function of the nominal layer thickness of deposited InAs. The solid line is for guiding the eye.

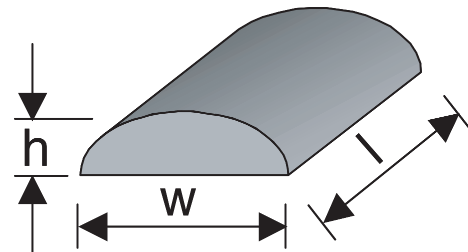

Figure 5. Schematic picture with the three major geometrical parameters height (h), width (w) and length (l) ($h \ll w \ll l$).

the dash density as well as the dot dimensions seems to be well preserved after overgrowth. Further details of growth parameters are reported in [40].

The optical properties and the application of such QDash layers in lasers and optical amplifiers will be discussed in the following paragraphs.

3. Basic properties of QDash layer structures

3.1. Optical properties of QDash layers

Low temperature PL spectra from QDash structures with a nominal InAs layer thickness of 1.3 nm (i.e. about 5 MLs) have luminescence energy at about 0.8 eV (1.5 μm). The exact emission wavelength is dependent on the growth parameters, e.g. the growth temperature, group-III/V ratio and growth rate. However, for the same growth parameters, control of the emission wavelength is high.

In figure 3, the PL spectra of QDash structures with different nominal InAs layer thicknesses are shown. All other growth parameters were the same. The linewidth of these emission lines are in the range of 35–50 meV, which is significantly less than for circular shaped dots grown on (001)B InP and indicates a low height variation. By changing the nominal layer thickness from 0.4 to 3.1 nm, equivalent to about 10 MLs, the emission wavelength can be continuously shifted by about 800 nm (cf figure 4). This material would allow an optical amplification between 1.2 and 2.0 μm.

The integrated PL intensity could be preserved between 0.6 and 1.9 nm (cf figure 3). Only above 3 nm, the intensity degrades significantly due to the creation of non-radiative recombination centres, presumably caused by partial strain relaxation.

To further extend the emission wavelength beyond 1.8 μm, an approach similar to that used for 1.3 μm QDs grown on GaAs is very useful [41], i.e. embedding by an GaInAs well. This dash-in-a-well (DWELL) concept also allows on InP substrates a reduction of the transition energy by lowering the barrier height of the QDash and supplying an additional In source during the dot formation process to avoid In depletion. With this concept, high performance QDash structures with emission wavelengths beyond 1.8 μm can be obtained, and laser operation at 1.88 μm (see below) and beyond 2 μm have already been demonstrated [42].

3.2. Theoretical considerations

Fundamental models were developed taking into account the specific geometry of QDashes. In figure 5, a schematic picture of a lens shaped single QDash structure is shown with three major geometrical parameters. To take into account the size fluctuation of dashes in real structures, the calculation of a single dash structure has to be kept rather simple to reduce the computing time. For that purpose, the lens-shape cross section of a dash structure was approximated by a rectangular one with an effective height and width [19]. The dominating dimension for the quantization energy is the height, h, of the structure, which is much smaller than the lateral dimensions, w and l. However, the dash width, w, about 20 nm, is small enough to lead to an additional quantization, while the dash extension in the third dimension is already large enough to build a miniband with indistinguishable states at room temperature. As a consequence, the QDash material behaves more as a quantum wire material with infinite dash length [18, 19]. However, the length of the dashes, about 50–100 nm, is still much shorter than the carrier diffusion length in bulk material. Therefore, the carrier localization in the lateral direction is very strong and QD specific effects like localized carrier recombination, local carrier storage or strongly reduced lateral carrier migration in the lateral directions [43] are expected to be observe in QDash material as well.

Based on this quantum mechanical model, macroscopic material properties, like luminescence spectra and material and modal gain of laser structures, can be calculated [19]. As an example, the ASE of a QDash SOA structure was calculated

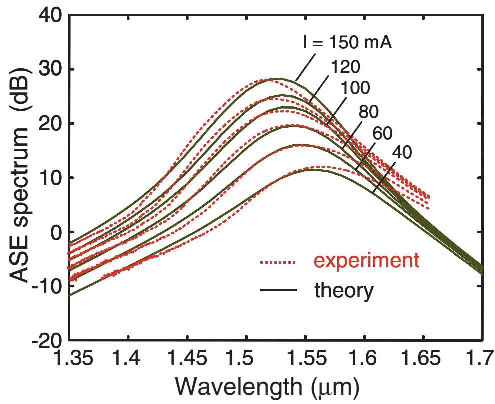

Figure 6. ASE spectra (· · · · · ·) of a QDash SOA structure with four stacked QDash layers operated at different injection currents as indicated. The solid lines are calculated ASE spectra taking into account an effective dash geometry deduced from measurements.

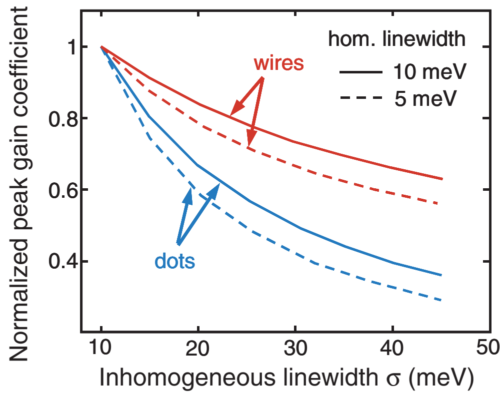

Figure 7. Comparison of the damping of the gain peak as a function of the inhomogeneous broadening, σ, between QDs and wires for two different homogenous linewidths (——: 10 meV, - - - -: 5 meV). The gain coefficient is normalized to the gain value of a dot/dash structure with 10 meV inhomogeneous linewidth.

and compared with measured spectra. In figure 6, the measured ASE spectra of a QDash SOA with four nominally identical QDash layers are shown for different operation currents (dotted lines). The simulation results (solid lines) are based on an effective dash geometry deduced from SEM and XTEM measurements. By fine-tuning of the size fluctuation, which is dominated by the height fluctuation, the ASE curves for different injection currents can only be fitted by assuming a wire-like geometry with about one order of magnitude longer extension in length than in width [19].

Although QDash structures are further away from an ideal low-dimensional system, they have some practical advantages beyond circular QDs. In particular, thanks to the QWire-like characteristics, the QDash gain is less sensitive to the size fluctuations with respect to a QD ensemble. For this purpose we compare in figure 7 the normalized peak gain, as a function of the inhomogeneous broadening, calculated for a QD and a QWire ensemble in the case of 5 meV (dashed line) and 10 meV (solid line) homogenous broadening [18]. We expect for the QDash material curves very similar to those for the QWire ones. For $\sigma = 10$–45 meV, the peak of the dot assembly gain coefficient drops by roughly two-thirds, whereas the reduction

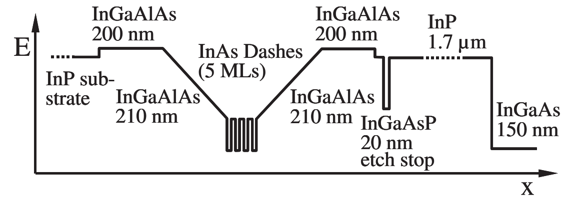

Figure 8. Schematic band structure of QDash laser design grown on (001) InP substrate. Growth direction is from left to right. All layers are lattice matched except the InAs dashes.

for the quantum wire case is only half that large. Also, for either assembly, a wider homogeneous broadening reduces the rate of reduction, as expected.

4. Lasers with dash-like active regions

4.1. Layer design

For the growth of laser structures presented in the following paragraphs, a GS-MBE system was used. Either a separate confinement heterostructure (SCH) or a graded index SCH (GRINSCH) design was used as the vertical waveguide. In figure 8, a sketch of a typical laser structure is plotted with a GRINSCH waveguide design and four stacked QDash layers at the centre. The internal structure consists of only phosphorus-free material to utilize the high conduction band offset between AlGaInAs and InAs ($\Delta E_c/\Delta E_g = 0.65$) in comparison with GaInAsP/InAs heterostructures ($\Delta E_c/\Delta E_g = 0.3$). For these layers a solid arsenic source was used. The upper InP cladding including the GaInAsP etch-stop layer and the InGaAs contact layer are grown by group-V gas sources. Different growth temperatures were used for the different compositions. The substrate temperatures for the different materials used range from 450˚C to 500˚C for InP and AlGaInAs, respectively. The GaInAs cap layer was grown at 460˚C, and the best results for the InAs dashes were obtained with a growth temperature of 485˚C.

4.2. Comparison between QDash and QWell lasers

In an earlier investigation, the performance of QWell and QDash lasers were directly compared. For that purpose, an SCH waveguide design with four active layers was used in both cases. In figure 9, the threshold current density values in dependence of the inverse cavity length are plotted for both types of lasers. The measurements were performed at room temperature in pulsed mode on broad area lasers with a 100 μm stripe width. Due to the reduced modal gain in QDash lasers caused by a finite dash-filling factor, the threshold current density of shorter devices is higher for QDash lasers than for QWell lasers. However, for longer devices, the inversion condition in QDash lasers, due to the reduced active material and increased density of state, is at lower current density values than for QWell lasers. As a consequence, the transparency current densities of QWell lasers could be reduced by introducing QDash layers by about a factor of 2 to an extrapolated value of about 350 A cm^{-2}.

Near the crossover point in the length dependence of the threshold current density (cf figure 9), the differential

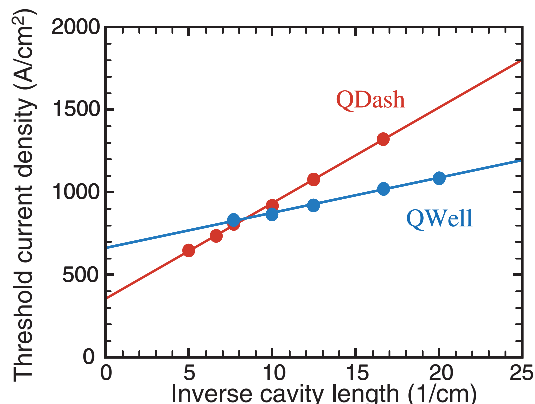

Figure 9. Threshold current density as a function of the inverse cavity length for QDash and QWell broad area lasers (100 μm width) with comparable waveguide design and four active layers. The lasers were operated in pulsed mode at room temperature.

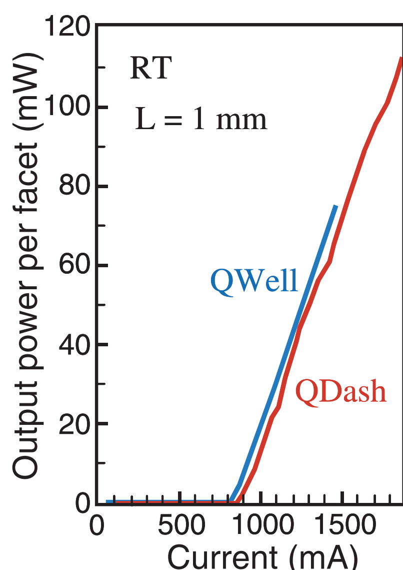

Figure 10. Light output characteristics of a QDash and QWell laser with an identical cavity length of 1 mm. The lasers were operated in pulsed mode at room temperature.

efficiency of QWell and QDash lasers is nearly identical. In figure 10, the light output characteristics of both types of lasers are plotted. For a cavity length of 1 mm and a stripe width of 100 μm a differential efficiency of 0.11 W A^{-1}/facet was obtained in these particular structures.

4.3. *Improved QDash laser designs*

With a stack of 4 nominally identical QDash layers, achieved by 25 nm thick barrier layers to avoid strain coupling [40], a net modal peak gain of about 10 cm^{-1} could be obtained at a current density of about 5 kA cm^{-2}. Such thick barriers, however, reduce the carrier collection efficiencies for the different dash layers. Therefore, a strong improvement can be achieved by reducing the barrier thickness. On reducing the barrier thickness to 10 nm, the strain coupling is already severe and the dash sizes increases on each subsequent dash layer. However, the improvement in modal gain is larger

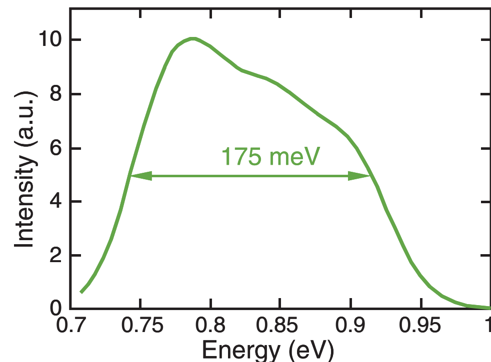

Figure 11. Calculated photoluminescence spectrum at $T = 8$ K of a QDash layer structure with four dash layers of different nominal thickness based on the theory described in the text.

and overcompensates the reduction due to additional spectral broadening. Gain measurements on laser structures with four strain coupled QDash layers and a barrier thickness of 10 nm achieve a net modal peak gain of more than 30 cm^{-1}. Details of the spectral gain function of broadband designs will be discussed in the next paragraph.

An additional significant improvement of the laser performance could be achieved by introducing a GRINSCH structure, as illustrated in figure 8, and by optimizing the doping profile. Recently developed waveguide designs for QDash lasers allow internal absorptions in the range of 3–5 cm^{-1} and quantum efficiencies above 60%. This leads to differential efficiencies in broad area lasers of 0.18 W A^{-1}/facet for 1 mm long devices [44]. The quantum efficiency values are already near the expected limits caused by intrinsic losses like Auger recombination, which is more severe on small bandgap materials. This could be shown for different dot laser systems [45, 46] and is not very much different from QWell lasers. Losses due to Auger recombination can only be significantly reduced by reducing the current density. Although low threshold current densities can be obtained with QD/QDash lasers, there are some limitations in the design to fulfilling also other specifications needed for applications like a sufficiently high modal gain to drive short devices, e.g. for high speed telecom applications.

4.4. *QDash lasers for broadband applications*

To further improve the gain bandwidth of QDash laser structures, combination of QDash layers of different nominal thickness is of interest. In figure 11, the simulation of the photoluminescence spectrum of a structure with four QDash layers of different nominal thickness is shown simulated by the model described in section 3.2. Due to the large inhomogeneous linewidth of each layer, a broad luminescence spectrum can be created without additional fine structures.

The calculated net modal gain for lasers with such a dash layer design is plotted in figure 12 (solid lines) for different injection current densities. In comparison with a dash layer design with four identical dash layers, the new dash design has a more homogeneously distributed gain over a wide spectral range. The peak gain, however, is significantly reduced by a factor of 3. Therefore, for real devices, a trade-off has to be made between spectral width and the minimum gain

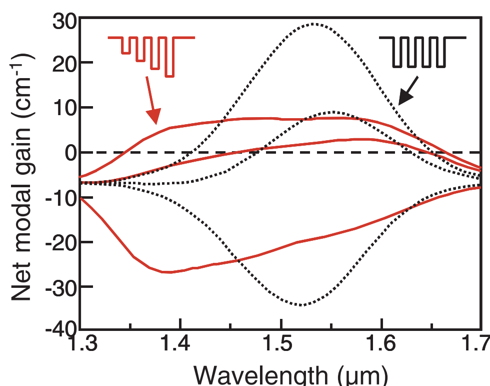

Figure 12. Calculated net modal gain of a laser with four identical QDash layers (······) and of different layers with different dash sizes (——) for different current densities well below, near and well above the threshold. The top-most curves correspond to about 3–5 kA cm^{-2}.

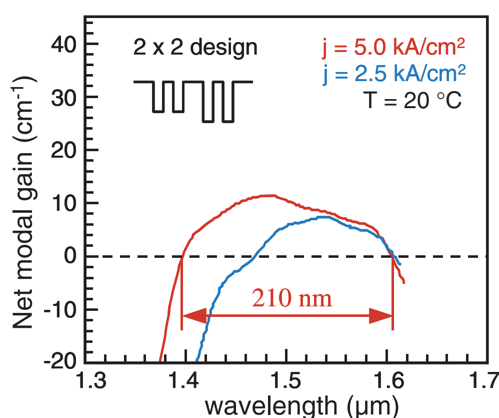

Figure 13. Modal net gain of a QDash laser with a broadened gain design consisting of two QDash layer groups of different nominal dash layer thicknesses. The individual QDash layers are separated by 10 nm and the groups by 20 nm, respectively. The measurements were performed by electroluminescence measurements on stripe contacts of different lengths at room temperature and determined at two different current densities.

necessary for driving the device. However, this optimization can especially be more easily obtained by QDash structures due to the flexibility in dash geometries and densities. As an example, two different QDash laser designs developed will be discussed in the following.

In figure 13, the measured net modal gain of a QDash laser with a 2 × 2 design is shown. Here, the active region consists of two groups of nominally identical QDash layers, each separated by a 10 nm barrier. The two groups are separated by a 20 nm barrier. Between the groups, the nominal QDash layer thickness was changed in order to manipulate the degree of gain inhomogeneity so as to increase the gain bandwidth. However, for a separation layer thicknesses below 30 nm, strain coupling occurs, which is most severe for the two subsequent layers in the growth sequence, which are separated by thinner, 10 nm, barriers. Strain coupling influences the dash formation process directly, resulting in larger dashes, i.e. lower transition energies, from layer to layer. As a consequence, the two QDash groups act as two independent inhomogenously broadened QDash structures of different average size. The net modal gain

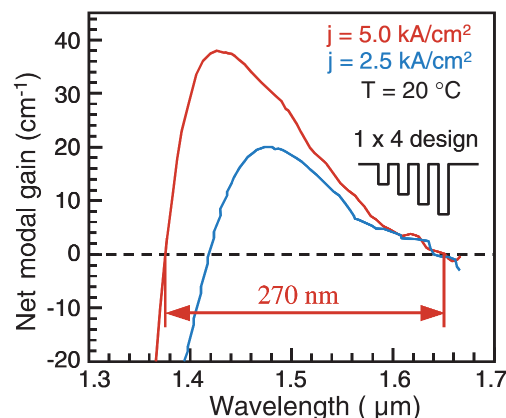

Figure 14. Modal net gain of a QDash laser with a broadened gain design consisting of four QDash layers with different dash sizes. The QDash layers are separated by 10 nm thick barriers.

is relatively flat. For a current density of 5 kA cm^{-2} a net peak gain of about 10 cm^{-1} and amplification over a bandwidth of 210 nm were obtained, comparable with the above-discussed calculations.

The gain profile of a second specialized design is shown in figure 14. Here, all four QDash layers have nominally different layer thicknesses and are separated by equal, thin, barriers of 10 nm width. Therefore, strain coupling leads to a further increase in the size distribution. In addition, QDashes placed several layers apart are most likely coupled electronically. This electronic coupling effect improves the carrier capture process significantly, yielding an increase in the peak gain up to nearly 40 cm^{-1} at 5 kA cm^{-2}. In addition, a wide gain bandwidth of 270 nm was obtained. This gain bandwidth is about a factor of 5 larger than typical bandwidths of QWell lasers.

By choosing an appropriate number of QDash layers with different sizes and controlling the strength of electronically coupling by different barrier thicknesses, the gain profile can be tailored over a wide spectral range suitable for different application purposes, e.g. an ultra-wide gain material with a flat gain profile.

4.5. QDash lasers with extended wavelengths

As shown in section 3.1 and figure 4, this QDash material system allows a wavelength adjustment over a wide spectral range. For lasers emitting beyond 1.7 μm, a DWELL structure is used to preserve a high optical quality in the QDash structures. In figure 15, the threshold current density is plotted as a function of the inverse cavity length, showing a low transparency current density comparable with that of the 1.5 μm emitting lasers. The emission wavelength is 1.88 μm at room temperature, which is very interesting for gas sensing applications, like the detection of water vapour. Rotter *et al* [42] demonstrated lasers with emission wavelengths up to 2.03 μm. Therefore, there is strong potential for this material system to cover a significant wavelength range for gas sensing purposes from 1.5 to beyond 2 μm.

4.6. Ridge waveguide lasers

Ridge waveguide (RWG) lasers were processed and high reflection (HR) coated at the reverse facet. In figure 16,

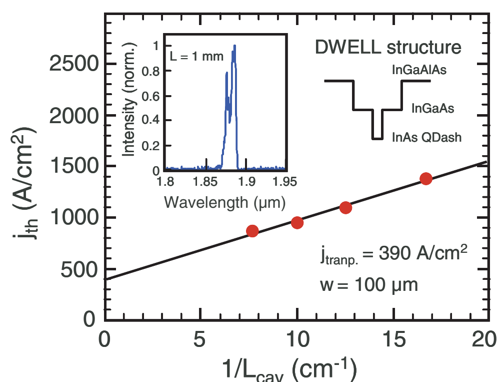

Figure 15. Threshold current density of a long wavelength broad area QDash structure with a DWELL design versus inverse cavity length. The inset shows the emission spectrum of a 1 mm long device.

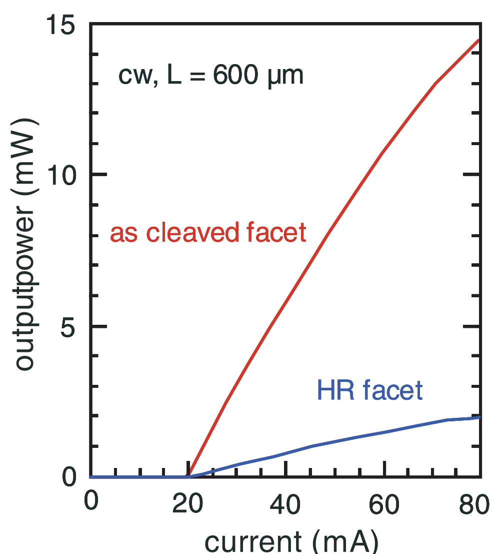

Figure 16. CW light output characteristics of a 600 μm long RWG QDash laser at 20°C. The laser facets are as-cleaved and HR coated. The QDash design is similar to the structure shown in figure 14.

the light output characteristics of a 600 μm long and 3 μm wide RWG laser are shown. The active region design is similar to the 1×4 design shown in figure 14, except that the nominal QDash thickness was not varied. However, due to strain coupling, an additional dash size variation occurs which broadens the gain profile. The net peak gain is nearly identical to the peak gain shown in figure 14, but the gain bandwidth is reduced to about 200 nm. With unmounted devices, a CW threshold current of 19 mA, a differential efficiency of about 0.32 W A^{-1} and a maximum output power of about 15 mW were obtained.

In figure 17, the temperature dependence of the light output characteristic of the same device is shown between 20°C and 110°C. Unmounted devices can also be driven by CW up to 75°C.

In longer RWG devices with as-cleaved facets, a cavity length of 2.5 mm and epi-side down mounting, a differential efficiency of 0.143 W A^{-1}/facet and a CW output power of 50 mW/facet were obtained in a single lateral mode [47]. These devices can be operated in CW beyond 85°C.

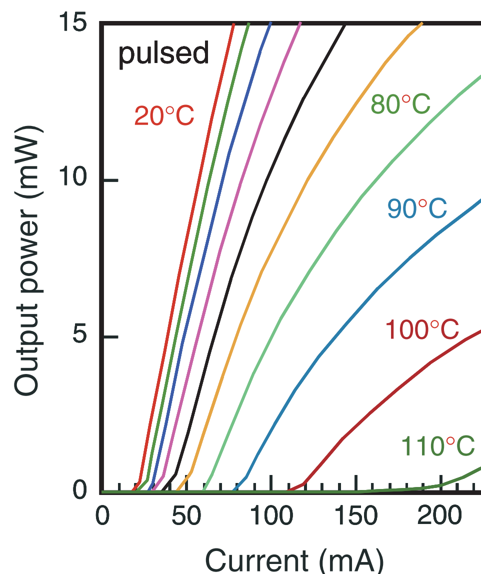

Figure 17. Temperature dependent light output characteristics of the same laser structure shown in figure 16 in pulsed operation.

4.7. Distributed feedback/distributed Bragg reflector lasers

For telecom applications, single mode emitting devices are necessary. For this purpose, distributed feedback (DFB) or distributed Bragg reflector (DBR) lasers with two different fabrication techniques were developed. One technique, described in more detail in [48], is based on a focused ion beam technique, where the grating is defined after a standard RWG process by direct implantation into the semiconductor lateral to the ridge and subsequent removal of the damaged area by a wet chemical etch technique. InP reacts in this process like an inorganic resist [49]. In addition, channelled ions are penetrating into the active region and initiate an intermixing of the QDash layers outside the RWG during an annealing step. Both effects together form a self-aligned complex grating consisting of the surface index grating and an underlying gain grating. DBR lasers with a 300 μm long grating and an 800 μm long gain section show a side-mode suppression ratio (SMSR) of more than 40 dB and a maximum single mode output power at room temperature of 30 mW [50].

The temperature dependence of QDash lasers is very different to that of QWell lasers. In figure 18, the temperature dependence of the emission wavelength of a Fabry–Perot and DBR QDash laser is compared with a QWell Fabry–Perot laser. While the QWell laser shows a temperature coefficient of $\Delta\lambda/\Delta T = 0.55$ nm K^{-1}, QDash lasers have a factor of about 3 reduced values. This low temperature dependence is already comparable with the refractive index change with temperature and allows the operation of DFB or DBR lasers over a much larger temperature range than possible with QWell material.

As a second approach, lateral metal gratings were used to obtain DFB lasers. This technique can be widely used for different material systems [51]. Due to the loss coupling, the SMSR is very high and the single-mode emission is very stable. In figure 19, the device characteristics of such a device are shown. The QDash DFB laser with a cavity length of 600 μm (same geometry as the RWG lasers shown in figure 16) has a threshold current of 30 mA, which is only slightly higher than

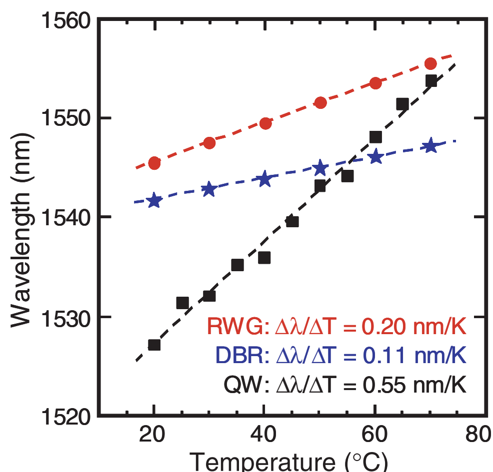

Figure 18. Temperature dependence of the emission wavelength for a QDash ridge wageguide (RWG, red dots), a distributed feedback (DBR, blue stars) and a QWell RWG laser (QW, black squares). The corresponding temperature coefficients are indicated. All measurements were done in pulsed operation.

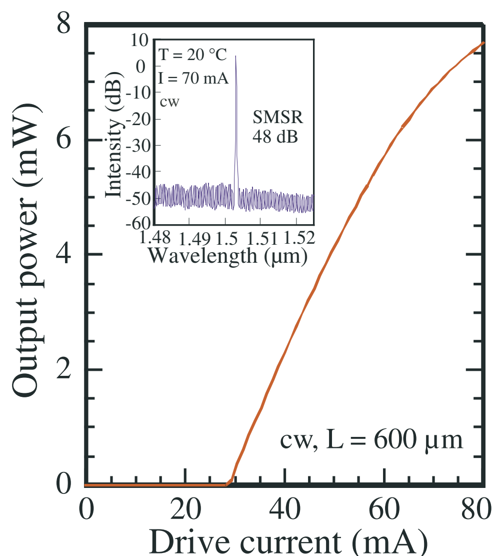

Figure 19. Light output characteristic of a 600 μm long QDash DFB laser at room temperature with lateral metal gratings. The inset shows the emission spectrum with an SMSR of 48 dB.

the RWG laser value. Due to the high wavelength selectivity of this complex coupled grating, an SMSR value of 48 dB was obtained (cf inset of figure 19).

4.8. High frequency properties

For telecom applications, the modulation speed is of great interest. Although a hybrid combination of a CW operating laser with a high speed modulator is often used to achieve a modulation speed of 10 GHz and well above, for low cost, high performance applications, there is a high demand for direct modulated lasers. Although the current QDash laser designs are not optimized for high speed direct modulation, a −3 dB bandwidth of 5.6 GHz could be determined for a 1 mm long RWG laser at a drive current of 60 mA (cf figure 20).

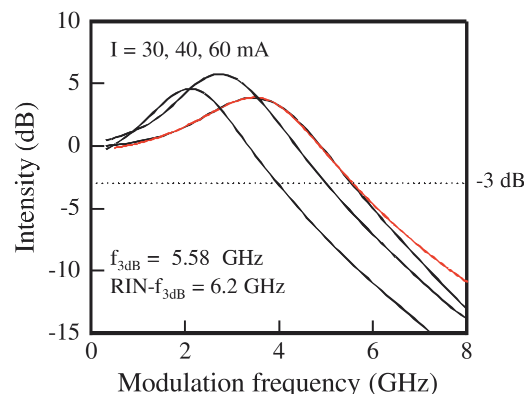

Figure 20. Small signal modulation transfer functions of a 1 mm long RWG laser operated at different CW drive currents. The red (on the right-hand side, top-most) curve is a fit using a standard damped oscillator function.

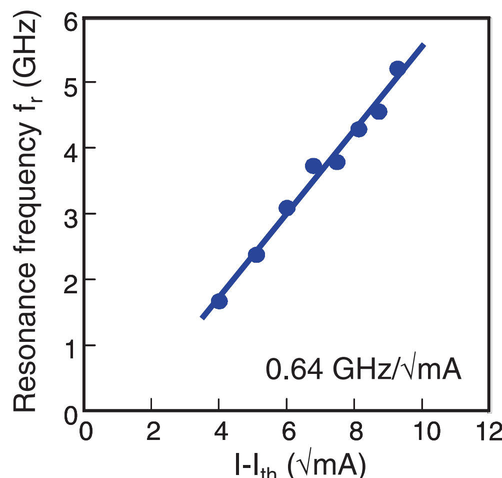

Figure 21. Resonance frequency values as a function of the square root of the injection current above the threshold determined by RIN measurements.

This value is not far away from the expected maximum modulation bandwidth of 6.2 GHz deduced from relative intensity noise (RIN) measurements.

The resonance frequency is plotted in figure 21 as a function of the square root of the drive current. A slope of 0.64 GHz per $\sqrt{\text{mA}}$ can be evaluated. At the maximum drive current, a resonance frequency of 5.2 GHz can be achieved.

The moderate modulation bandwidth is consistent with detailed modelling we have performed [52, 53], which describes the dynamic limitations of nanostructure lasers stemming from both the inhomogenous broadening and the state filling effect. The model [52] shows that the differential gain and the non-linear damping cannot be optimized simultaneously. Indeed, this fact causes the bandwidth of QD and QDash lasers based on conventional heterostructures (including the laser presented here) to be below 10 GHz and to exhibit high damping.

However, the high damping leads to a very important property—low RIN operation under CW conditions. The RIN spectrum of a 2.5 mm long QDash laser is shown in figure 22 [47]. The noise level of this device is extremely

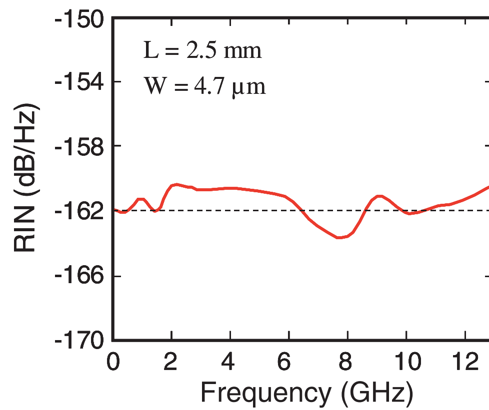

Figure 22. Noise spectrum for a 2.5 mm long and 4.7 μm wide RWG QDash laser in CW operation at an output power of 40 mW/facet. The noise level is about 10–15 dB Hz^{-1} lower than for comparable QWell lasers.

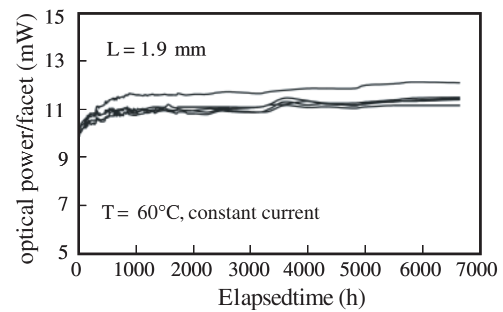

Figure 23. Lifetime measurements of RWG QDash lasers of 1.9 mm cavity length. The lasers were operated in constant current mode and at 60°C junction temperature.

low. A noise level below -160 dB Hz^{-1} is about 10–15 dB lower than that of the best QWell lasers. In addition, this low noise level is nearly flat over a large spectral range between 0.1 and 13 GHz and is achieved by a multi-mode Fabry–Perot laser without wavelength selection. These device properties are very interesting, e.g. for ultra-low noise light sources for microwave data links.

To overcome the current restrictions for the modulation speed, intrinsic limitations have to be considered, like the combined effects of a finite capture time of carriers into the QDashes and carrier escape, the gain inhomogenity and the hole transport time. Detailed theoretical studies [52] and experimental confirmation [54] were performed to simulate the role of the discrete energy states of QDashes with finite barrier heights and their interaction with continuum states of the wetting layer (WL) for the carrier capture process. It was shown that the symmetry between the capture and escape processes of hot carriers in general limits the response time of such a system to a frequency range of the order of 10 GHz or below because the differential gain and non-linear gain compression coefficient cannot be optimized simultaneously. This effect is not unique to QDash structures. Also the modulation speed of 1.3 μm InAs/GaAs QD lasers is limited to about 10 GHz [55, 56].

An additional limiting effect, common to all nanostructures (QDs, wires and wells) placed in a standard heterostructure, is the finite room temperature carrier occupation of excited, barrier and WL states. This so-called state filling effect [53] dictates that the maximum differential gain, and hence the modulation bandwidth, is almost identical for all such nanostructure-based lasers [53].

Different approaches are feasible for improving the modulation speed of QD lasers. Some improvement of the differential gain can be achieved by p doping of the active region. The influence of p doping was simulated in the case of different QDash laser designs with different barrier thicknesses and with/without a WL [57]. The conclusions are that a minor doping concentration is important for obtaining a significant increase in the differential gain if the barrier is thin (e.g. <40 nm). However, the presence of the WL significantly reduces the effectiveness of p-type doping on the differential gain. Therefore, only p doping without improving the carrier confinement, i.e. increasing the potential depth of the QDs, is not sufficient.

A more promising approach is based on tunnel injection, which was first shown in quantum wells [58] and later on in short wavelength QD lasers as well [59]. By injecting electrons through an adjacent quantum well into a higher order QD/dash state, hot electron effects like carrier escape out of the dots/dashes can be suppressed and much faster capture times can be expected. In combination with a moderate p doping, which allows us to overcome the hole transport bottleneck, tunnel injection should allow us to increase significantly the differential gain and the bandwidth.

4.9. Reliability properties

In general, strained material systems near the critical thickness for relaxation can be sensitive to the creation of crystal defects, which can act as non-radiative recombination centres. However, strained layers in the pseudomorphic regime are more robust against misfit dislocation movements in a crystal than in unstrained material. In QDs or QDashes, the highly strained material is three-dimensionally embedded in material, which is lattice matched to the substrate. Therefore, the strain can be more easily accommodated by the matrix material, which increases the threshold for the creation of crystal defects. In comparison with InAs dots grown on GaAs, we expect much less problems in the case of InAs dashes grown on InP due to only half of the lattice mismatch.

To prove this assumption, reliability measurements were performed on 1.9 mm long RWG devices. In figure 23, the lifetime measurements of five devices are shown over a time period of 6500 h. The lasers are operated in constant current mode with an output power of about 10 mW/facet and at a pn junction temperature of 60°C. After a burn-in within the first 100–200 h, the lasers are very stable, with a slight improvement in output power with time.

5. Semiconductor optical amplifiers

A major interest in QD/dash material in the telecom wavelength range is the expected high speed properties based on the much faster gain recovery in comparison with quantum well or bulk amplifiers [60–62]. In addition, there were predictions of the possibility of amplifying several wavelengths without cross

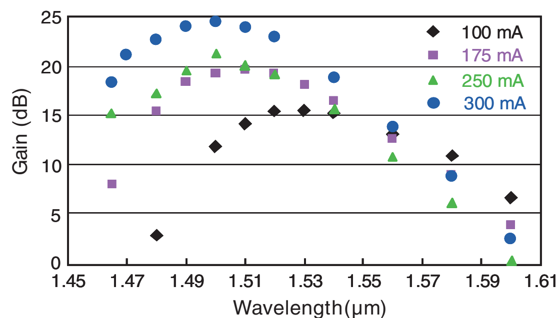

Figure 24. Optical gain spectra of a 2.5 mm long and 3.5 μm wide QDash SOA for different drive currents. A maximum chip gain of 25 dB was obtained at a drive current of 300 mA.

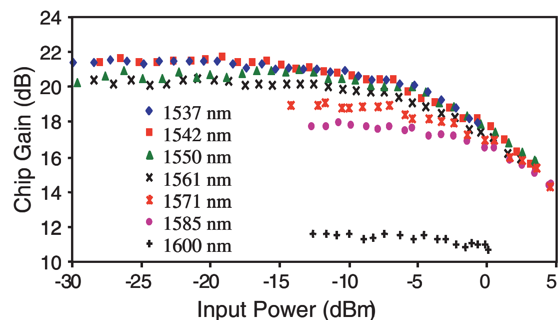

Figure 25. Output power of a QDash SOA with 2.5 mm device length as a function of the input power and wavelength. At 0 dBm input power, a saturation output power of 18 dBm can be obtained.

talk at the same time and increasing the saturation output power. Parts of these predictions were already confirmed on 1.3 μm QD amplifiers [63, 64].

From the fabrication point of view, semiconductor amplifiers are processed similar to RWG lasers, except for high quality anti-reflection (AR) coated facets for avoiding any cavity feedback. The SOA results presented in the following are RWG lasers with a typical lateral waveguide geometry of 3–5 μm width and 1–2.5 mm length. The QDash design is identical to the laser structures shown above. The facet was cleaved in the $[0-11]$ direction parallel to the dash orientation and perpendicular to the ridge. A broadband AR coating was used to cover a wavelength range of more than 200 nm with a reflectivity below 10^{-3} and a minimum reflectivity better than 10^{-4}.

5.1. Static properties

In figure 24, the optical gain spectra of a 2.5 mm long SOA is shown for different drive currents. With a drive current of 300 mA, a bandwidth of 120 nm at a chip gain of 10 dB can be obtained, which is about three times broader than the bandwidth of a QWell SOA. In figure 25, the chip gain as a function of the input power is plotted for different wavelengths. For these measurements the in- and out-coupling losses are in the range of 6 dB, which was taken into account to get the chip gain. The QDash SOA has a very flat amplification characteristic over a large input power range. At 0 dBm input power a saturation output power of 18 dBm can be achieved, which is in comparison with QWell SOAs a very high value

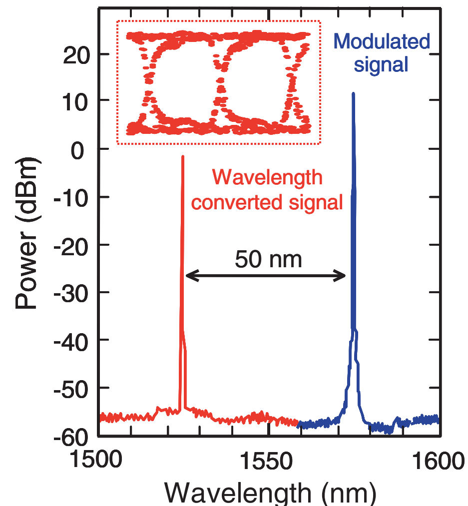

Figure 26. Spectrum of modulated input signal (right side in blue) and wavelength converted output signal (left side in red). The eye-diagram of a 2.5 GBit s^{-1} wavelength converted PRB signal is shown in the inset.

and confirms the predicted high saturation power due to the spatially distributed optical gain, the fast recovery time and the small confinement factor.

5.2. Wavelength conversion

In contrast to the limited modulation bandwidth of direct modulated laser diodes, much faster response characteristics are expected in optical amplification by using QD/dash structures due to their local carrier storage and lesser dependence on the carrier capture process. In addition, due to the spatially separated carrier recombination and strong inhomogenous gain broadening, no cross talk for different wavelength regions is expected, which should allow multi-wavelength amplification.

Since different regions across the gain spectrum are partially coupled through the WL, some cross coupling is possible. It turn out that this cross coupling is bit rate dependent due to the specific dynamics of carrier capture and escape [54].

Experiments to test wavelength conversion by cross-gain modulation in a QDash SOA are described in figure 26. The spectra of a modulated input pump signal (right-hand side spectrum) and of a 50 nm wavelength shifted CW test signal (left-hand side spectrum), which is modulated by the input signal during the transmission through the SOA, are shown. As can be seen in the inset of figure 26, the converted signal shows an open eye for a pseudo random bit (PRB) stream at a speed of 2.5 GBit s^{-1}. Therefore, this QDash SOA act as a perfect wavelength converter up to wavelength shifts of the order of half of the bandwidth and up to moderate modulation frequencies. For longer wavelength shifts or much higher modulation frequencies, the wavelength-converted signal vanishes.

5.3. Multi-wavelength and high speed amplification

At higher modulation rates, multi-wavelength amplification is possible and was demonstrated for the first time in QDash

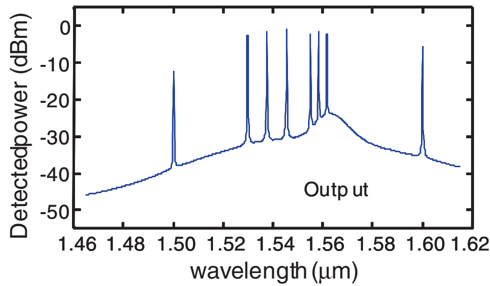

Figure 27. Optical output spectrum of a QDash SOA with eight simultaneously amplified input signals at different wavelengths. An input power of −21 dBm was used for all eight wavelengths. Each PRB signal is modulated at a data rate of 10 GBit s^{-1}.

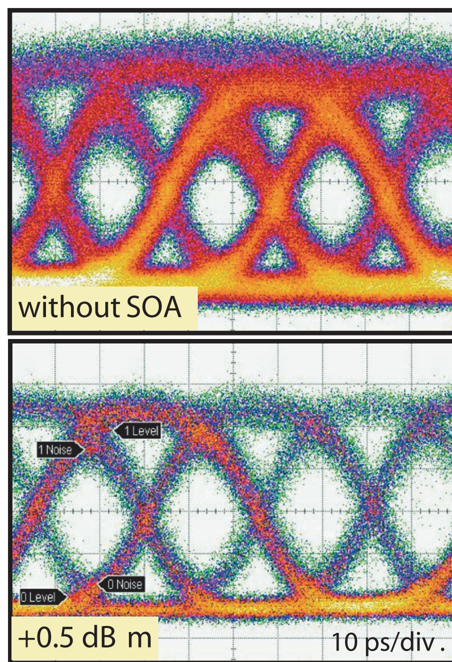

Figure 28. Sampling oscilloscope graphs of a 40 GBit s^{-1} input signal (top) and of the amplified signal (bottom) at an input power of 0.5 dBm. The QDash SOA is driven in deep saturation, which improves the extinction ratio significantly.

SOAs [65]. In figure 27, the output signals of eight different amplified wavelength channels are shown. Each of the channels is modulated with a data rate of 10 GBit s^{-1}. At that speed, no cross talk between the channels could be observed in bit-error measurements.

High speed transmission experiments were performed by time domain multiplexing of four 10 GBit s^{-1} signals to create a 40 GBit s^{-1} bit stream. In figure 28, a sampling oscilloscope graph of the input signal (on top) and of the amplified output signal is shown (bottom). No pattern effect can be observed within the whole amplification power range from low power up to deep saturation at 0.5 dBm input power. As can be seen in the widely open eye diagram of the amplified signal in figure 28, the quality factor (i.e. eye opening) can be significantly improved after amplification by operating the SOA in the saturation condition. Further details on the noise and dynamic properties of QD and QDash SOAs are discussed in [66].

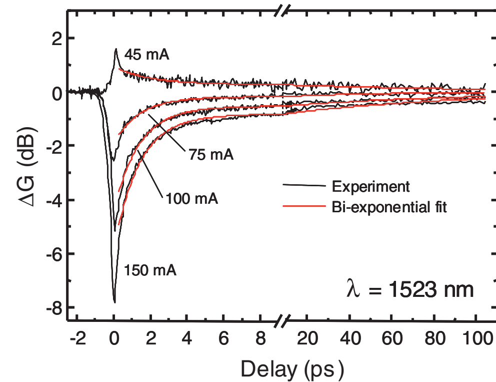

Figure 29. Time resolved spectra of the gain change in a QDash SOA at different drive currents. The test signal has a wavelength of 1523 nm and a pulse length of 150 fs.

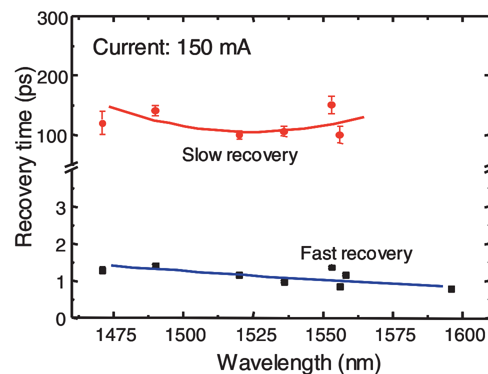

Figure 30. Time constants of the gain recovery of QDash SOAs as a function of the wavelength distinguished between a fast (bottom) and slow (top) component. The device was operated with 150 mA drive current.

5.4. High speed dynamics

A better understanding of the complex carrier and recombination dynamics in QDash structures can be gained by time resolved spectroscopy. In figure 29, the fast time response characteristics of a QDash SOA are shown for different operation conditions. Here, the gain change is plotted after testing the device by a 150 fs probe pulse and at a wavelength of 1523 nm, which is near the gain maximum. The SOA reacts very fast within less than 1 ps rise-time and about 1–2 ps recovery time [67]. In addition to this fast recovery time, there is a slow component, as can be seen in the bi-exponential fit in figure 29, of the order of 100–200 ps.

The recovery time is weakly wavelength dependent. In figure 30, the two time constants are plotted as function of the probe wavelength. The fast recovery time seems to slightly increase for shorter wavelengths, while the slow recovery time stays constant.

Based on these time resolved measurement results and theoretical considerations, one can develop a simple picture, which explain the major dynamic effects in QDash SOAs and lasers. In QDash SOAs, a very fast response can be achieved by the local storage of carriers within each dash. In this case, the larger density of states in dashes in comparison with smaller circular dots has the advantage that more carriers can be locally stored. This time constant is illustrated in figure 31 on the

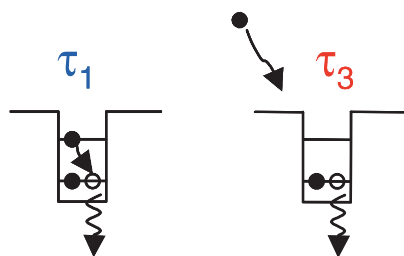

Figure 31. Illustration of two possible time constants in QDot/QDash structures. Left-hand side, intra-dot relaxation; right-hand side, carrier capture through WL states.

very left (τ_1). As long as enough carriers can be fed into the dots within the pulse length, no signal distortion will occur. In deep saturation, the extinction ratio might be reduced, however, as experimentally shown in figure 28, the extinction ratio at 40 GBit s^{-1} is only slightly reduced, although the device was driven in deep saturation.

By direct modulation of lasers, the output signal is directly related to the carrier capture process as illustrated on the right-hand side of figure 31 (τ_3). The time constant of 100–200 ps is in agreement with the observed modulation bandwidth discussed in section 4.7. However, this slow component is also responsible for a considerable cross talk between the dashes through the continuum states of the WL. This is the reason why for low modulation frequencies, as shown in the cross-gain modulation experiment, spatially separated dots of different sizes and transition energies are electronically coupled. At higher frequencies, this coupling is too weak and only the fast component dominates. Further related details on the dynamics of dot/wire like structures are reported in the literature [53, 68–70].

6. Summary and conclusions

Different self-assembly techniques are possible for fabricating dot- or dash-like structures on InP substrates for long wavelength applications. A brief review of the different technologies and their current status has been given. In terms of device performance, QDash structures have several advantages at the present stage of development. The most important point is the high dash density and the related high modal gain. Also, the large dash size in comparison with circular dots allows storing more carriers in one dot. Therefore, gain recovery in optical amplifiers can be very fast at high saturation conditions.

A more detailed report was given about the fabrication of QDash laser structures using InAs dashes on AlGaInAs surfaces lattice matched to (001) InP substrates. This dash-formation process is very flexible and allows a wavelength variation between 1.2 and 2 μm only by changing the number of deposited InAs MLs. As a consequence, there is a large freedom in designing a gain material with a tailored spectral gain profile. With different QDash layers a gain bandwidth of 270 nm was achieved. The obtained laser performance already has device quality with a high differential gain ($>$0.35 W A^{-1}) and low threshold current ($<$20 mA for 600 μm long RWG laser). Maximum operation temperatures beyond 100˚C in pulsed mode and up to 75˚C in CW were demonstrated. Lifetime measurements up to 6500 h at 60˚C without failures demonstrate a high reliability. Internal resonance frequencies of more than 5 GHz could be measured on standard structures not optimized for high speed direct modulation. However, to allow modulation speeds beyond 10 GHz, new design approaches have to be used, like tunnel injection structures and p doping.

Most of the device properties of lasers can be theoretically treated as the laser consists of a wire-like gain material. Nevertheless, dot-like properties, like local carrier recombination and spectrally inhomogenously distributed gain, are still preserved and lead to extraordinary properties of optical amplifiers, like multi-wavelength amplification (eight wavelengths demonstrated without cross-talk) and very fast recovery times of 1 ps. However, the dynamics seems very complex, because contradictory behaviour occurs. Although multi-wavelength amplification at high modulation frequencies can be achieved, wavelength conversion with large wavelength differences is observed at lower modulation frequencies. The major reason is the balance between different time scales related to fast intra-dot relaxation and slow carrier capture times. However, more detailed studies are necessary to understand the complex interaction of all different states involved, especially highly localized dot states and continuum states in the WL or barriers.

Acknowledgments

We would like to thank A Sauerwald, T Kümmell and G Bacher, University of Duisburg for XTEM investigations, Y Robert, M Carbonnelle and C Dernazaretian, Thales R&T in Orsay and M Wagenbrenner, A Wolf, H Schuller and M Emmerling, Microstructure Laboratory of University of Würzburg for excellent technical assistance and the financial support by the European Community through the IST project BigBand.

References

[1] Arakawa Y and Sakaki H 1999 Multidimensional quantum well laser and temperature dependence of its threshold current *Appl. Phys. Lett.* **40** 939–41

[2] Asada M, Miyamoto Y and Suematsu Y 1986 Gain and the threshold of three dimensional quantum-box lasers *IEEE J. Quantum Electron.* **22** 1915–21

[3] Liu G T, Stintz A, Li H, Malloy K J and Lester L F 1999 Extremely low room-temperature threshold current density diode lasers using InAs dots in In0.15Ga0.85As quantum well *Electron. Lett.* **35** 1163–5

[4] Shchekin O B, Park G, Huffaker D L, Mo Q and Deppe D G 2000 Low-threshold continuous-wave two-stack quantum-dot laser with reduced temperature sensitivity *IEEE Photon. Technol. Lett.* **12** 1120–2

[5] Mukai K, Nakata Y, Otsubo K, Sugawara M, Yokoyama N and Ishikawa H 2000 1.3 μm CW lasing characteristics of self-assembled ingaas–gaas quantum dots *IEEE J. Quantum. Electron.* **36** 472–8

[6] Klopf F, Deubert S, Reithmaier J P and Forchel A 2002 Correlation between the gain profile and the temperature-induced wavelength-shift of quantum dot lasers *Appl. Phys. Lett.* **81** 217–19

[7] Schäfer F, Reithmaier J P and Forchel A 1999 High-performance GaInAs/GaAs quantum-dot lasers based on a single active layer *Appl. Phys. Lett.* **74** 2915–17

[8] Huffaker D L, Park G, Zhou Z, Shchekin O B and Deppe D G 1998 1.3 μm room-temperature GaAs-based quantum dot laser *Appl. Phys. Lett.* **73** 2564–6

[9] Shernyakov Y M *et al* 1999 1.3 μm GaAs-based laser using quantum dots obtained by activated spinodal decomposition *Electron. Lett.* **35** 898–9

[10] Ledentsov N N *et al* 2003 High performance quantum dot lasers on GaAs substrates operating in 1.5 μm range *Electron. Lett.* **39** 1126–8

[11] Li H, Daniels-Race T and Hasan M-A 2002 Effects of the matrix on self-organization of InAs quantum nanostructures grown on InP substrates *Appl. Phys. Lett.* **80** 1367–9

[12] Fafard S, Wasilewski Z, McCaffrey J, Raymond S and Charbonneau S 1996 InAs self-assembled quantum dots on InP by molecular beam epitaxy *Appl. Phys. Lett.* **68** 991–3

[13] Brault J, Gendry M, Grenet G, Hollinger G, Olivares J, Salem B, Benyattou T and Bremond G 2002 Surface effects on shape, self-organization and photoluminescence of InAs islands grown on InAlAs/InP(001) *J. Appl. Phys.* **92** 506–10

[14] Stintz A, Rotter T J and Malloy K J 2003 Formation of quantum wires and quantum dots on buffer layers grown on InP substrates *J. Cryst. Growth* **255** 255–72

[15] Ustinov V M *et al* 1998 Low threshold quantum dot injection laser emitting at 1.9 μm *Electron. Lett.* **34** 670–2

[16] Li Y F, Liu F Q, Xu B, Ye X L, Ding D, Sun Z Z, Jiang W H, Liu H Y, Zhang Y C and Wang Z G 2000 Two-dimensional ordering of self-assembled InAs quantum dots grown on (3 1 1)B InP substrate *J. Cryst. Growth* **219** 17–21

[17] Frechengues S, Bertru N, Drouot V, Lambert B, Robinet S and Loualizhe S 1999 Wavelength tuning of InAs quantum dots grown on (311)B InP *Appl. Phys. Lett.* **74** 3356–8

[18] Dery H, Benisty E, Epstein A, Alizon R, Mikhelashvili V, Eisenstein G, Schwertberger R, Gold D, Reithmaier J P and Forchel A 2004 On the nature of quantum dash structures *J. Appl. Phys.* **95** 6103–11

[19] Gioannini M 2004 Numerical modelling of the emission characteristics of semiconductor quantum dash materials for lasers and optical amplifiers *IEEE J. Quantum Electron.* **40** 364–73

[20] Nötzel R, Fukui T, Hasegawa H, Temmyo T and Jamamura T 1994 Atomic force microscopy study of strained InGaAs quantum disks self-organizing on GaAs (n11)B substrates *Appl. Phys. Lett.* **65** 2854–6

[21] Poole P J, McCaffrey J, Williams R L, Lefebvre J and Chithrani D 2001 Chemical beam epitaxy growth of self-assembled InAs/InP quantum dots *J. Vac. Sci. Technol.* B **19** 1467–70

[22] Ponchet A, Le Corre A, L'Haridon H, Lambert B and Salaun S 1995 Relationship between self-organization and size of InAs islands on InP(001) grown by gas-source molecular beam epitaxy *Appl. Phys. Lett.* **67** 1850–2

[23] Nishi K, Yamada M, Anan T, Gomyo A and Sugou S 1998 Long-wavelength lasing from InAs self-assembled quantum dots on (311) B InP *Appl. Phys. Lett.* **73** 526–8

[24] Saito H, Nishi K and Sugou S 1999 Low-threshold lasing from high-density InAs quantum dots of uniform size *Electron. Lett.* **35** 1561–3

[25] Miska P, Even J, Parantheon C, Dehaese O, Folliot H, Loualiche S, Senes M and Marie X 2003 Optical properties and carrier dynamics of InAs/InP(113)B quantum dots emitting between 1.3 and 1.55 μm for laser applications *Physica* E **17** 56–9

[26] Paranthoen C *et al* 2003 Growth and optical characterizations of InAs quantum dots on InP substrate: towards a 1.55 μm quantum dot laser *J. Cryst. Growth* **251** 230–5

[27] Mori J, Nakano T, Shimada T, Hasegawa S and Asahi H 2004 Wavelength control of 1.3–1.6 μm light emission from the quantum dots self-formed in GaAs/InAs short-period superlattices grown on InP (411)A substrates *J. Appl. Phys.* **96** 1373–5

[28] Saito H, Nishi K and Sugou S 2001 Ground-state lasing at room temperature in long-wavelength InAs quantum-dot lasers on InP (311)B substrates *Appl. Phys. Lett.* **78** 267–9

[29] Salem B, Olivares J, Guillot G, Bremond G, Brault J, Monat C, Gendry M, Hollinger G, Hassen F and Maaref H 2001 Optical properties of self-assembled InAs quantum islands grown on InP(001) vicinal substrates *Appl. Phys. Lett.* **79** 4435–7

[30] Lefebvre J, Poole P J, Aers G C, Chithrani D and Williams R L 2002 Tunable emission from InAs quantum dots on InP nanotemplates *J. Vac. Sci. Technol.* B **20** 2173–6

[31] Jeong W G, Dapkus P D, Lee U H, Yim J S, Lee D and Lee B T 2001 Epitaxial growth and optical characterization of InAs/InGaAsP/InP self-assembled quantum dots *Appl. Phys. Lett.* **78** 1171–3

[32] Allen C N, Poole P J, Marshall P, Fraser J, Raymond S and Fafard S 2002 InAs self-assembled quantum-dot lasers grown on (100) InP *Appl. Phys. Lett.* **80** 3629–31

[33] Borgstrom M, Pires M P, Bryllert T, Landi S, Seifert W and Souza P L 2003 InAs quantum dots grown on InAlGaAs lattice matched to InP *J. Cryst. Growth* **252** 481–5

[34] Qiu Y, Uhl D, Chacon R and Yang R Q 2003 Lasing characteristics of InAs quantum-dot lasers on (001) InP substrate *Appl. Phys. Lett.* **83** 1704–6

[35] Qiu Y and Uhl D 2003 Effect of thin GaAs interface layer on InAs quantum dots grown on InGaAs/InP using metalorganic vapor phase epitaxy *J. Cryst. Growth* **257** 225–30

[36] Kim J S, Lee J H, Hong S U, Han W S, Kwack H S, Lee C W and Oh D K 2004 Room-temperature operation of InP-based InAs quantum dot laser *IEEE Photon. Technol. Lett.* **16** 1607–9

[37] Wang R H, Stintz A, Varangis P M, Newell T C, Li H, Malloy K J and Lester L F 2001 Room-temperature operation of InAs quantum-dash lasers on InP (001) *IEEE Photon. Technol. Lett.* **13** 767–9

[38] Schwertberger R, Gold D, Reithmaier J P and Forchel A 2002 Long wavelength InP based quantum dot lasers *IEEE Photon. Technol. Lett.* **14** 735–7

[39] XTEM charaterization was performed by Sauerwald A, Kümmell T, Bacher G, Werkstoffe der Elektrotechnik, Universitát Duisburg-Essen

[40] Schwertberger R, Gold D, Reithmaier J P and Forchel A 2003 Epitaxial growth of 1.55 μm emitting InAs quantum dashes on InP-based heterostructures by GS-MBE for long-wavelength laser applications *J. Cryst. Growth* **251** 248–52

[41] Stintz A, Liu G T, Li H, Lester L F and Malloy K J 2000 Low-threshold current density 1.3 μm InAs quantum-dot lasers with the dots-in-a-well (DWELL) structure *IEEE Photon. Technol. Lett.* **12** 591–3

[42] Rotter T J, Stintz A and Malloy K J 2003 InP based quantum dash lasers with 2 μm wavelength *IEE Proc.-Optoelectron.* **150** 318–21

[43] Popescu D P, Eliseev P G, Stintz A and Malloy K J 2003 Carrier migration in structures with InAs quantum dots *J. Appl. Phys.* **94** 2454–8

[44] Somers A, Kaiser W, Reithmaier J P, Forchel A 2005 InP based quantum dash lasers for broadband optical amplification and gas sensing applications *Indium Phosphide and Related Compounds Conf.* (Glasgow, May 2005)

[45] Marko I P, Andreev A D, Adams A R, Krebs R, Reithmaier J P and Forchel A 2003 The role of Auger recombination in InAs 1.3 μm quantum-dot lasers investigated using high hydrostatic pressure *IEEE J. Sel. Top. Quantum Electron.* **9** 1300–7

[46] Marko I P, Sweeney S J, Adams A R, Jin S R, Murdin B N, Schwertberger R, Somers A, Reithmaier J P and Forchel A 2004 Recombination mechanisms in InAs/InP quantum dash lasers studied using high hydrostatic pressure *Phys. Status Solidi* b **241** 3427–31

[47] Resneau P, Bansropun S, Calligaro M, Krakowski M, Schwertberger R, Somers A, Reithmaier J P and Forchel A 2004 High power and low noise 1.55 μm InP-based quantum dash lasers *Photonics Europe (Strasbourg, France, April 2004)* paper 5452-03

[48] Bach L, Rennon S, Reithmaier J P and Forchel A 2002 Laterally coupled DBR laser emitting at 1.55 μm fabricated by focused ion beam lithography *IEEE Photon. Technol. Lett.* **14** 1037–9

[49] König H, Reithmaier J P and Forchel A 1999 Highly resolved maskless patterning on InP by focused ion beam enhanced wet chemical etching *Japan. J. Appl. Phys.* **38** 6142–4

[50] Bach L, Kaiser W, Schwertberger R, Reithmaier J P and Forchel A 2003 1.54 μm single mode InP-based Q-dash lasers *Electron. Lett.* **39** 985–7

[51] Kamp M, Hofmann J, Forchel A, Schäfer F and Reithmaier J P 1999 Low threshold high quantum efficiency laterally gain coupled InGaAs/AlGaAs distributed feedback lasers *Appl. Phys. Lett.* **74** 483–5

[52] Dery H and Eisenstein G 2004 Self-consistent rate equations of self-assembly quantum wire lasers *IEEE J. Quantum Electron.* **40** 1398–409

[53] Dery H and Eisenstein G 2005 The impact of energy band diagram and inhomogeneous broadening on the optical differential gain in nanostructure lasers *IEEE J. Quantum Electron.* **41** 26–35

[54] Bilenca A, Alizon R, Mikhelashhvili V, Dahan D, Eisenstein G, Schwertberger R, Gold D, Reithmaier J P and Forchel A 2003 Broad-band wavelength conversion based on cross-gain modulation and four-wave mixing in InAs–InP quantum-dash semiconductor optical amplifiers operating at 1550 nm *IEEE Photon. Technol. Lett.* **15** 563–6

[55] Kim S M, Wang Y, Keever M and Harris J S 2004 High-frequency modulation characteristics of 1.3 μm InGaAs quantum dot lasers *IEEE Photon. Technol. Lett.* **16** 377–9

[56] Arakawa Y 2004 Quantum-dot laser has temperature-independent operation *Laser Focus World* **40** 9

[57] Gioannini M 2004 Investigation of p-type doping effect on the gain characteristics of quantum dash semiconductor lasers *SPIE Proc.* **5452** 562–33

[58] Bhattacharya P, Singh J, Yoon H, Zhang X, Gutierrez-Aitken A and Lam Y 1996 Tunnelling injection lasers: a new class of lasers with reduced hot carrier effects *IEEE J. Quantum Electron.* **32** 1620–9

[59] Ghosh S, Praghan S and Bhattacharya P 2002 Dynamic characteristics of high-speed InGaAs/GaAs self-organized quantum dot lasers at room temperature *Appl. Phys. Lett.* **81** 3055–7

[60] Berg T W, Bischoff S, Magnusdottir I and Mørk J 2001 Ultrafast gain recovery and modulation limitations in self-assembled quantum-dot devices *IEEE Photon. Technol. Lett.* **13** 541–3

[61] Sugawara M, Hatori N, Akiyama T, Nakata Y and Ishikawa H 2001 Quantum-dot semiconductor optical amplifiers for high bit-rate signal processing over 40 GBit s^{-1} *Japan. J. Appl. Phys.* **40** L488–91

[62] Berg T W and Mørk J 2004 Saturation and noise properties of quantum-dot optical amplifiers *IEEE J. Quantum Electron.* **40** 1527–39

[63] Borri P, Langbein W, Hvam J M, Heinrichsdorff E, Mao M H and Bimberg D 2000 Ultrafast gain dynamics in InAs-InGaAs quantum-dot amplifiers *IEEE Photon. Technol. Lett.* **12** 594–6

[64] Akiyama T, Nobuaki H, Nakata Y, Ebe H and Sugawara M 2003 Pattern-effect-free amplification and cross-gain modulation achieved by using ultrafast gain nonlinearity in quantum-dot semiconductor optical amplifiers *Phys. Status Solidi.* b **238** 301–4

[65] Alizon R *et al* 2004 Multiple wavelength amplification in wide band high power 1550 nm quantum dash optical amplifier *Electron. Lett.* **40** 760–1

[66] Bilenca A and Eisenstein G 2004 On the noise properties of linear and nonlinear quantum-dot semiconductor optical amplifiers: the impact of inhomogeneously broadened gain and fast carrier dynamics *IEEE J. Quantum Electron.* **40** 690–702

[67] van der Poel M *et al* 2005 Measurements of gain and index dynamics in quantum dash semiconductor optical amplifiers *OSA Conference on Optical Amplifiers and their Applications (San Francisco, USA, June 2004)* paper OTuD4

[68] Hadass D *et al* 2004 Spectrally resolved dynamics of inhomogeneously broadened gain in InAs/InP 1550 nm quantum-dash lasers *Appl. Phys. Lett.* **85** 5505–7

[69] Sugawara M, Ebe H, Hatori N, Ishida M, Arakawa Y, Akiyama T, Otsubo K and Nakata Y 2004 Theory of optical signal amplification and processing by quantum-dot semiconductor optical amplifiers *Phys. Rev.* B **69** 235332 1–39

[70] Uskov A, Berg T W and Mørk J 2004 Theory of pulse-train amplification without patterning effects in quantum-dot semiconductor optical amplifiers *IEEE J. Quantum Electron.* **40** 306–20